Letters in Applied NanoBioScience
Open-Access Journal (ISSN: 2284-6808)

Article
Volume 15, Issue 1, 2026, 27
https://doi.org/10.33263/LIANBS151.027

Thermal Radiation Impact on MHD Nanofluid Flow through a Concentric Cylinder Concerning Cancer Therapy

Mahesha Rudrappa [1], Sravan Kumar Thavada [1,*], Nalinakshi Narasappa [1], Sreevallaba Reddy A

[1] Department of Mathematics, Atria Institute of Technology, Bengaluru-560024, Visvesveraya Technological University, Belagavi-590018, KA, India
[2] Department of Mathematics, M S Ramaiah Institute of Technology, Bangalore 560 054, Karnataka, India
* Correspondence: sravan.k@atria.edu;

Received: 5.11.2024; Accepted: 25.02.2026; Published: 30.03.2026

Abstract: The aim of the current study is to analyze heat transfer in horizontal two concentric cylinders in the influence of MHD, internal heat source/sink containing porous nanofluids, and thermal radiation are considered. The impact of internal heat source/sink and porous media of H_2O-Cu nanofluids on the influence of the Lorentz effect is analyzed; its applications are cooling systems and heat exchangers. Furthermore, a transformation of the momentum and energy equations was applied in this study to obtain a set of ODEs for the basic governing equations in heat transfer flows. In addition, applying the numerical technique of the BVP4C method to solve a system of non-linear, coupled equations with boundary conditions. The influence of Hartmann number, volume fraction, radiation parameter, internal heat source/sink parameter, Darcy number, and different nanoparticles is examined in velocity and temperature profiles. The results reveal that thermal radiation significantly influences the temperature distribution within the annulus, thereby affecting the heat transfer rate. Moreover, the presence of the porous medium and internal heat source/sink modulates the flow patterns. This study provides optimization of MHD nanofluid systems for engineering applications in thermal management, hyperthermia treatment in cancer therapy, food processing, rotating machinery, and cooling systems. The results are in good agreement with the existing work on velocity and temperature graphs.

Keywords: MHD; internal heat source/sink; porous and nanofluid medium; thermal radiation.

1. Introduction

Heat transfer is the process of transforming heat energy into mechanical energy to improve the efficiency of heat transfer; it becomes a challenging issue in industrial and engineering applications. To analyze the effective heat transfer, the presence of nanofluids plays a role in cooling/heating effects. The fluid properties of nanofluids, such as thermal conductivity, viscosity, and stability, are high, which play an important role in industrial applications. Firstly, Choi and Eastman [1] investigated nanofluid behavior in heat transfer analysis. Mixed convection is the convection of both natural and forced, investigated by Merkin *et al.* [2]. Natural convection from a vertically flat heated plate in the presence of an external

hydromagnetic field, with heat and mass transfer, is examined by Ali *et al*. [3]. Stability analysis flow of magnetic field investigated numerically by Gurejala *et al.* [4].

A numerical analysis of free convection MHD over a moving vertical flat plate using Lie group transformation was examined by Md. Uddin *et al.* [5]. Heat and mass transfer analysis of free convection in the presence of MHD, radiation, and heat generation/absorption over a stretching sheet, as explained by Ali et al. [6]. As a result, the boundary layer thickness increases with an increase in viscosity. Finite element analysis and simulation of a steady case over a cylinder in the impact of hydromagnetic forces are investigated by [7,8], resulting in magnetic forces that oppose the fluid rate. Different nanoparticles are analyzed. Heat transfer analysis of unsteady, non-Newtonian, MHD flow in a contracting cylinder and a numerical method explained by Saranya and Al-Mdallal [9]. As a result, MHD advances fluid flow rate, and $CoFe_2O_4$ nanofluid dominates the fluid flow system. The effect of non-linear electrified jets in the electrospinning process is analyzed using the bead-spring model investigated by Vahidi *et al.* [10]. The simulations of non-Newtonian rheology observed that elongation dynamics reduce the stable jet length. Besthapu *et al*. [11] explained thermal radiation, MHD of Casson nanofluid flow over a stretching surface of convective stagnation point, which gives the Sherwood number, demonstrating the significant influence of Brownian motion, and solved Keller's box techniques.

MHD is an electrically conducting fluid in the presence of a magnetic field. MHD flow and heat transfer by shrinking a permeable sheet of nanofluids are explained by Valipour and Gouran *et al.* [12]. As a result, with an increasing volume fraction temperature profile of skin friction, the Nusselt number increases. Saranya and Al-Mdallal [13] investigated the numerical analysis of hybrid nanofluids of ferroparticles in a cylinder using the Legendre Collocation method for unsteady viscous-ohmic dissipative effects. Heat transfer rate and skin friction coefficient decrease with Eckert number. A comparative analysis of exact and numerical techniques for the accuracy of the non-linear vibration of single-walled carbon nanotubes using the nonlocal Timoshenko beam theory, as examined by Ghasemi and Ranjbar [14], shows that the frequency of the single-walled carbon nanotubes' amplitude increases. Ghasemi and Gouran [15] examined the motion of vertically nano droplets in incompressible Newtonian fluids using analytical and numerical techniques. As a result, the effect of sphericity on velocity and acceleration is analysed. Natural convection of Cu-water-based nanofluids between two infinite parallel plates is examined by Dehghani *et al*. [16], which gives thermal boundary layer thickness decreases with increasing volume fraction.

A comparative analysis of analytical and numerical techniques by a rigid rod in a circular surface, examined by Gouran *et al.* [17], shows that oscillation amplitude decreases and velocity is maximum at 60°. Influence of nonlocal parameters, high velocity observed in a theoretical analysis of single-walled carbon nanotubes is analysed by Vahidi *et al*. [18] using the Pasternak-type model. A temperature-dependent heat transfer analysis of solid and porous convective fins with different effects, such as thermal conductivity and heat generation, is performed using a semi-analytical method [19, 20], resulting in higher efficiency. Talarposhti *et al*. [21] investigated the analytical Exp-function method to solve the sine-Gordon and Ostrovsky equations of the wave equation. The method is efficient and plots contour plots for velocity profiles. Nanofluid flow in two concentric cylinders of different thermal conductivities, MHD, thermal radiation effect, investigated by Sheikholeslami *et al*. [22]. The results show that temperature enhances the Eckert number and Reynolds number. Sohail *et al*. [23] investigated heat and mass transfer mathematical analysis of a non-linear stretching

surface in gyrotactic microorganisms using Brownian and thermophoresis effects. The results show that the magnetic parameter retard the fluid flow rate. Sohail and Naz [24] examined heat and mass transfer in MHD over a stretching cylinder, solving it using exact and numerical techniques. It gives the results of escalating values of the magnetic parameter in the velocity profile.

An interesting work is reported by Ghasemi and Hatami [25], analysing solar radiation and MHD with nanofluids over a stretching surface using the numerical differential quadrature method, which yields a more accurate solution, and showing that the thermal boundary layer thickness increases with the Biot number. The influence of the magnetic field of the nanofluid in a hot cylinder is solved by a numerical method. As a result, the Lorentz force causes a fluid flow system to be investigated by Sheikholeslami [26, 27], and forced convection Fe_3O_4-Ethylene Glycol-based nanofluid heat transfer is analyzed. Theoretical analysis of two parallel porous blocks between micropolar fluid is investigated by Valipour *et al.* [28], using analytical and numerical methods, which gives good results, with a high magnitude of the microrotation velocity. Gouran *et al.* [29] examined the theoretical analysis of MHD, solar radiation between two concentric cylinders, which results in the Nusselt number enhancing the radiation, and the Hartmann number. Heat transfer analysis of rotating horizontal annulus in the influence of MHD, thermal radiation is examined by Peng *et al.* [30], and using a thermal conductivity model, it is found that as a result, the Hartmann number decreases fluid flow rate. Investigation of variable fluid properties of mixed convection MHD over a vertical heated plate with a porous matrix by a numerical method; as a result, the magnetic field diminishes the fluid flow rate [32 - 40].

Based on the above literature survey, many authors have failed to analyse heat transfer between two concentric rotating cylinders, taking into account internal heat generation, MHD, thermal radiation, and a nano-porous medium. The impact of internal heat generation is seen in industry and engineering applications, such as cooling of nuclear reactors, MHD generators, thermal control systems, rotating heat exchangers, solar energy systems, chemical reactors, hyperthermia treatment for cancer therapy, nanofluidic drug delivery, and thermal management in medical devices. A comparative analysis of different thermal-conductivity models enhances heat transfer to destroy targeted cancer cells. Microscale catheters or probes inserted into tumours, where nanofluid flow with controlled heating by radiation and magnetic field leads to cell death by elevating local tissue temperature.

2. Materials and Methods

2.1. Mathematical formulation.

Consider steady, laminar, incompressible, unidirectional fluid flow of a two concentric cylinder Cu-H_2O nanofluid, as shown in Figure 1. By assuming the induced magnetic field is ignored, the Lorentz force is applied along the fluid flow. Impact of internal heat generation/absorption, thermal radiation, over two concentric cylinders containing nano with porous medium. The radial axis acts upwards, and fluid flow along the z-axis with T_1 is the temperature for r_1, T_2 is the temperature for r_2, between two cylinders containing porous nanofluids. In this current problem, the governing equations of Cu-H_2O nanofluids and heat transfer in a cylindrical coordinate system with boundary conditions [22, 30] are given by:

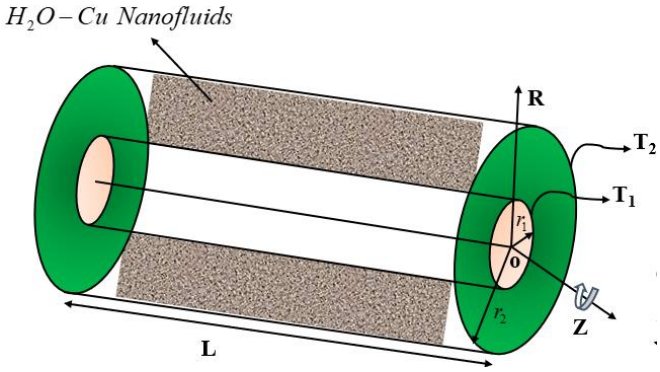

Figure 1. Physical configuration flow problem.

Conservation of mass:

$$\frac{1}{R}\left(\frac{\partial}{\partial R}(UR)\right) = 0 \qquad (1)$$

Conservation of momentum:

$$\upsilon_{nf}\left(\frac{\partial^2 U}{\partial R^2} + \frac{1}{R}\frac{\partial U}{\partial R} - \frac{U}{R^2}\right) - \frac{\sigma_{nf} U B_0^2}{\rho_{nf}} - \frac{U\mu_{nf}}{k\rho_{nf}} = U\frac{\partial U}{\partial R} \qquad (2)$$

Conservation of energy:

$$\frac{\kappa_{nf}}{R}\frac{\partial}{\partial R}\left(R\frac{\partial T}{\partial R}\right) + \mu_{nf}\left(\frac{\partial U}{\partial R} - \frac{U}{R}\right)^2 - \frac{\partial q_r}{\partial R} - Q_0(T - T_2) = \left(\rho C_p\right)_{nf} U\frac{\partial T}{\partial R} \qquad (3)$$

The boundary conditions are imparted:

$$R = r_2 : U(R) = 0, T = T_2,\ R = r_1 : U(R) = \omega r_1, T = T_1 \qquad (4)$$

Using the Taylor series expansion and Rosseland approximation, the heat flux rate of radiation is given by:

$$T^4 \cong 4T_2^3 T - 3T_2^4,\ q_r = -\frac{4\sigma_e}{3\beta_R}\frac{\partial T^4}{\partial R},\ \frac{\partial q_r}{\partial R} = -\frac{4\sigma_e 4T_2^3}{3\beta_R}\frac{\partial^2 T}{\partial R^2} \qquad (5)$$

The modified energy equation using equation (5) in equation (3) is given by:

$$\frac{\kappa_{nf}}{R}\frac{\partial}{\partial R}\left(R\frac{\partial T}{\partial R}\right) + \mu_{nf}\left(\frac{\partial U}{\partial R} - \frac{U}{R}\right)^2 + \frac{4\sigma_e 4T_2^3}{3\beta_R}\frac{\partial^2 T}{\partial R^2} - Q_0(T - T_2) = \left(\rho C_p\right)_{nf} U\frac{\partial T}{\partial R} \qquad (6)$$

The non-dimensional analysis of the above governing equations [22, 30] is:

$$r = \frac{R}{r_2},\ u = \frac{U}{\omega r_1},\ \eta = \frac{r_1}{r_2},\ \theta = \frac{T - T_2}{T_1 - T_2} \qquad (7)$$

The non-dimensional parameters are Reynolds number, Prandtl number, Eckert number, Thermal radiation, Hartmann number, Darcy number, Internal heat source/sink parameter, and thermophysical properties.

$$Re = \frac{\rho_f \omega r_1 r_2}{\mu_f}, Pr = \frac{\mu_f (\rho C_p)_f}{\rho_f \kappa_f}, Ec = \frac{\rho_f (\omega r_1)^2}{(\rho C_p)_f \Delta T}, N = \frac{4\sigma_e T_c^3}{\beta_R \kappa_f}, Ha = B_0 d \sqrt{\frac{\sigma_f}{\mu_f}}, Da = \frac{k}{r_2^2} Q = \frac{Q_0 r_2^2}{\kappa_f}, S_1 = \frac{\rho_{nf}}{\rho_f}, S_2 = \frac{\mu_{nf}}{\mu_f}, S_3 = \frac{(\rho C_p)_{nf}}{(\rho C_p)_f}, S_4 = \frac{\kappa_{nf}}{\kappa_f}, S_5 = \frac{\sigma_{nf}}{\sigma_f}, \eta = \frac{r_1}{r_2} \quad (8)$$

Apply the non-dimensional transformation equations (7) to the above equations (1-2) and equations (4, 6) using equations (8) and Table 1 [31] to form non-dimensional equations:

$$\frac{\partial^2 u}{\partial r^2} + \frac{1}{r}\frac{\partial u}{\partial r} - \left\{\frac{Ha^2}{(1-\eta^2)}\frac{S_5}{S_2} + \frac{1}{r^2}\right\} u - \frac{u}{Da} - Re\frac{S_1}{S_2} u \frac{\partial u}{\partial r} = 0 \quad (9)$$

$$\frac{\partial^2 \theta}{\partial r^2} + \frac{1}{r}\frac{\partial \theta}{\partial r} + Ec\, Pr \frac{S_2}{S_4}\left\{\frac{\partial u}{\partial r} - \frac{u}{r}\right\}^2 + \frac{4}{3}\frac{N}{S_4}\frac{\partial^2 \theta}{\partial r^2} - \frac{Q}{S_4}\theta - PrRe\frac{S_3}{S_4} u \frac{\partial \theta}{\partial r} = 0 \quad (10)$$

Dimensionless boundary conditions imparted:

$$r = \eta: u = 1, \theta = 1$$
$$r = 1: u = 0, \theta = 0 \quad (11)$$

Table 1. Thermophysical properties of spherical-shaped nanofluids [31].

Properties	Formulas
Heat capacitance	$(\rho C_p)_{nf} = (1-\phi)(\rho C_p)_f + \phi(\rho C_p)_s$
Thermal expansion coefficients	$(\rho\beta)_{nf} = (1-\phi)(\rho\beta)_f + \phi(\rho\beta)_s$
Thermal diffusivity	$\alpha_{nf} = \frac{\kappa_{nf}}{(\rho C_p)_{nf}}$
Density variation	$\rho_{nf} = (1-\phi)\rho_f + \phi\rho_s$
Dynamic viscosity	$\mu_{nf} = \frac{\mu_f}{(1-\phi)^{2.5}}$
Thermal conductivity	$\kappa_{nf} = \kappa_f\left(\frac{2\kappa_f - 2\phi(\kappa_f - \kappa_s) + \kappa_s}{2\kappa_f + \phi(\kappa_f - \kappa_s) + \kappa_s}\right)$

The micro convection relation introduced by Patel *et al.*. [34], the effective TC for nanofluid is:

$$\left.\begin{aligned} \frac{\kappa_{nf}}{\kappa_f} &= 1 + \frac{\kappa_s A_s}{\kappa_f A_f} + c\kappa_s P_e \frac{A_s}{\kappa_f A_f} \\ \frac{A_s}{A_f} &= \frac{d_f}{d_s}\frac{\phi}{1-\phi} \\ P_e &= \frac{u_s d_s}{\alpha_f}, u_s = \frac{2k_B T}{\pi \mu_f d_s^2}, c = 25{,}000 \end{aligned}\right\} \quad (12)$$

We associate the effective dynamic viscosity as [34]:

$$\mu_{nf} = \mu_f(1 + 39.11\phi + 533.9\phi^2) \quad (13)$$

Non-dimensional Skin friction and Nusselt number are given by:

$$C_f = -S_2 \frac{\partial u}{\partial r}\Big|_{r=\eta} \quad Nu = -S_4\left(1 + \frac{4N}{3S_4}\right)\frac{\partial \theta}{\partial r}\Big|_{r=\eta} \quad (14)$$

2.2. Methodology.

The dimensionless flow problem is non-linear and coupled equations with boundary conditions of equations (– 9 - 11) are solved numerically by the BVP4C method using MATLAB software. By employing this method, to form the set of 1st order ODE's such as $y_1 = r, y_2 = u, y_3 = u', y_4 = \theta, y_5 = \theta'$. The algorithm and corresponding to the boundary conditions are:

$$\begin{pmatrix} y_1' \\ y_2' \\ y_3' \\ y_4' \\ y_5' \end{pmatrix} = \begin{pmatrix} 1 \\ y_3 \\ \frac{-y_3}{y_1} + \frac{y_2}{y_1} + \frac{Ha^2}{(1-\eta^2)}\frac{S_5}{S_2}y_2 + \frac{y_2}{Da} + \frac{Re\,S_1}{S_2}y_2 y_3 \\ y_4 \\ \frac{1}{\left(1+\frac{4}{3}\frac{N}{S_4}\right)}\left(\frac{-y_5}{y_1} - \frac{Ec\,Pr\,S_2}{S_4}\left(y_3 - \frac{y_2}{y_1}\right)^2 + \frac{Qy_4}{S_4} + \frac{PrRe\,S_3 y_2 y_5}{S_4}\right) \end{pmatrix} \quad (15)$$

And related boundary conditions are $\begin{pmatrix} y_1 \\ y_2 \\ y_3 \\ y_4 \\ y_5 \end{pmatrix} = \begin{pmatrix} \eta \\ 1 \\ u' \\ 1 \\ \theta' \end{pmatrix}$.

To obtain a convergent solution, initial estimates for unknown parameters such as $y_1 = r, y_2 = u, y_3 = u', y_4 = \theta, y_5 = \theta'$ are arbitrarily chosen. These estimates are refined iteratively using the BVP4C method, which provides numerical approximations with high accuracy. The iterative procedure also involves determining an appropriate maximum value of η, ensuring that the asymptotic conditions $R = r_1 : U(R) = \omega\, r_1, T = T_1$ $R = r_2 : U(R) = 0, T = T_2$ are satisfied. A trial-and-error approach is used to refine the guesses for unknowns, followed by an iterative correction process to meet the convergence criteria. The error tolerance is set to 10^{-6} to ensure numerical stability and accuracy. For all computations, a step size of $\Delta\eta = 0.01$ is used, balancing computational efficiency with solution accuracy.

Table 2. Numerical values of physical properties of Water and different nanoparticles.

Property	Water	Ag	Cu	CuO
$\rho(kgm^{-3})$	997.1	10500	8933	6320
$\mu(Pas)$	0.00089	-	-	-
$\kappa(Wm^{-1}K^{-1})$	0.613	429	401	76.5
$\beta \times 10^{-5}(K^{-1})$	21	1.89	1.67	1.80
$C_p(Jkg^{-1}K^{-1})$	4179	235	305	531.8
$\sigma(\omega m)^{-1}$	5.5×10^{-6}	6.3×10^{-7}	5.8×10^{-7}	1×10^{-6}

3. Results and Discussion

The non-dimensional equations of (9 - 11) are solved numerically using the BVP4C method with a set of first-order ODEs using MATLAB software, Table 2 [31], dimensionless BC's, and plotted the velocity and temperature graphs keeping parameters constant, such as $\phi = 0.01,\ Pr = 6.8,\ \eta = 0.5,\ Re = 1, Ec = 0.01, R = 0.1,\ Da = 1,\ Q = 1,\ Ha = 1.$

3.1. Effect of volume fraction (ϕ).

From Figure 2, we observe that an increasing volume fraction velocity increases, which is due to increasing density and viscosity, leading to a reduction in the resistance of the fluid

flow system, and dispersion of nanoparticles in fluid causes a strong buoyancy force. It is useful in a heat exchanger system. In Figure 3, we can analyze volume fraction behaviors in the temperature profile. Temperature decreases as solid volume fraction increases. This is because the addition of nanoparticles with higher thermal conductivity increases the nanofluid's overall thermal conductivity, facilitating more efficient heat transfer to its surroundings, promoting uniform heat dispersion, and reducing temperature. Its applications are in electronic cooling systems and automotive cooling engine systems.

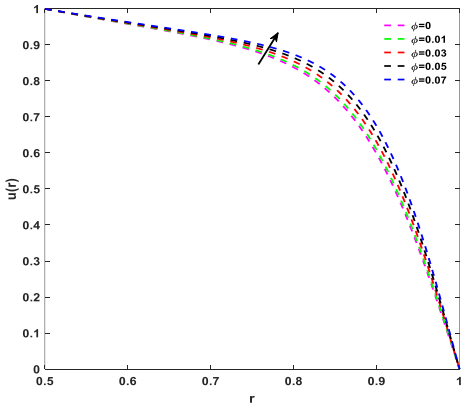

Figure 2. Variation of ϕ on velocity.

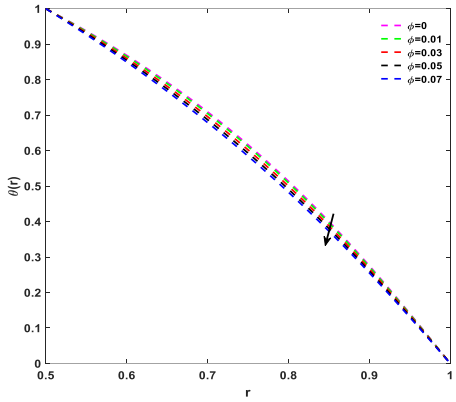

Figure 3. Variation of ϕ on temperature.

3.2. Effect of Hartman number (Ha).

Figures 4 and 5 visualize the effect of magnetic force on velocity and temperature plots.

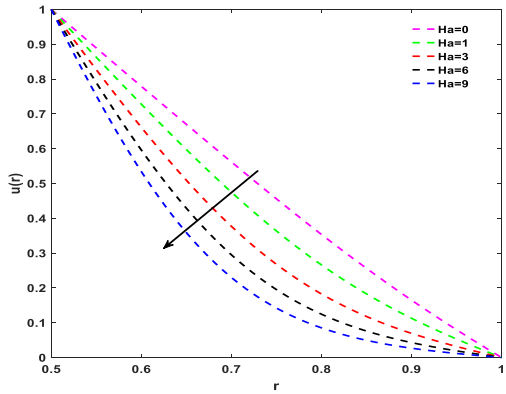

Figure 4. Variation of Ha with velocity.

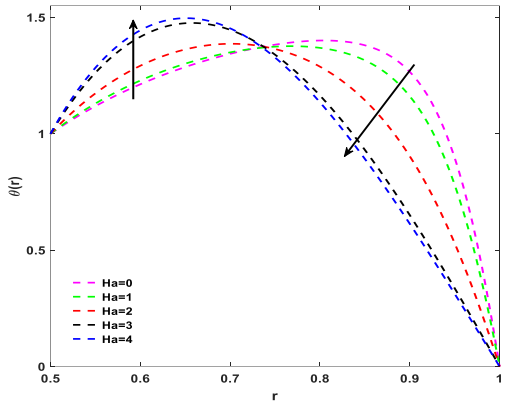

Figure 5. Variation of Ha with temperature.

An increase in the Hartmann number decreases the velocity and temperature, due to the Lorentz force dominating the viscous force and the Lorentz force damping effect. The temperature profile (Figure 5) in a concentric-cylinder system initially increases due to heat transfer from the heated inner cylinder by conduction, and weak convection dominates. As the radial distance increases, the fluid absorbs more heat until it reaches a maximum point. Beyond this peak, the temperature decreases because the combined effects of magnetic damping (due to the Lorentz force), radiative heat loss, and reduced fluid motion near the outer cylinder limit further heat transport. The intersection point of the temperature curves for different Hartmann numbers (Ha) indicates a shift from magnetic effects that enhance heat retention near the inner cylinder to those that suppress heat transport farther out. This behaviour is significant in hyperthermia-based cancer therapy, where targeted heating near the tumour (inner cylinder) and cooling near healthy tissues (outer cylinder) is desired. Even though the convective heat transfer rate drops and the suppression of fluid flow leads to a reduction in the thickness of the thermal boundary layer, it is useful in MHD pumps and MHD flow control.

3.3. Effect of internal heat source parameter (Q) and viscous dissipation (Ec).

Figure 6 shows temperature versus the internal heat source parameter. An increase in the heat source parameter temperature occurs because adding thermal energy to the system increases molecular motion, which in turn increases temperature gradients. This is seen in applications such as circuit analysis in electronic devices. The effect of viscous dissipation on temperature is analyzed in Figure 7. As the Eckert number increases, the temperature rises due to the domination of kinetic energy in fluid flow, which converts to thermal energy. This may lead to increased viscosity and the generation of internal heat, which is useful in hydrodynamic bearings.

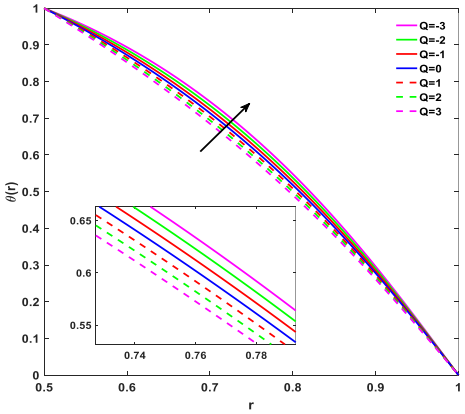

Figure 6. Variation of Q with temperature.

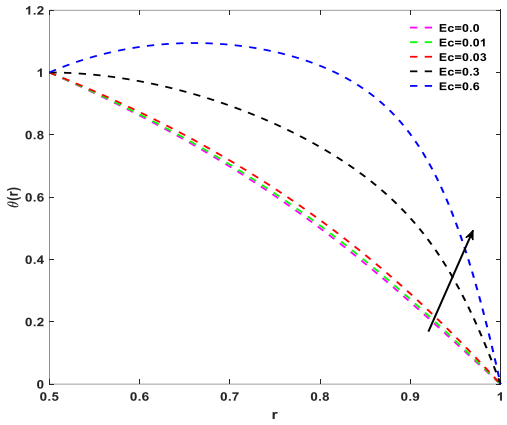

Figure 7. Variation of Ec with temperature.

3.4. Effect of Darcy number (Da).

Variation of Darcy number is analyzed in Figures 8 and 9, where an increasing Darcy number, velocity, and temperature are observed. In the velocity profile, understand that the application of efficient filtration processes, due to the presence of a porous matrix that increases permeability, allows large-pore fluid flow to occur easily, resulting in increased resistance and pressure drops. Simultaneously, in the temperature graph, heat transfer increases due to the higher flow rate and the reduced thermal resistance from the internal heat source, which is useful for geothermal energy extraction.

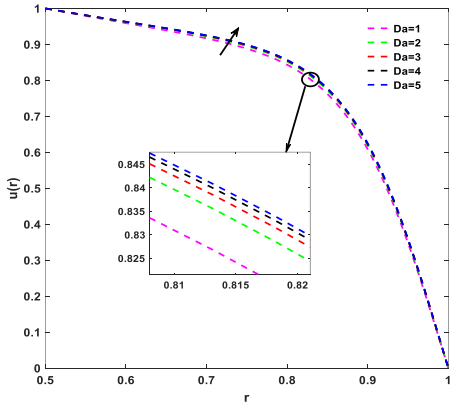

Figure 8. Variation of Da on velocity.

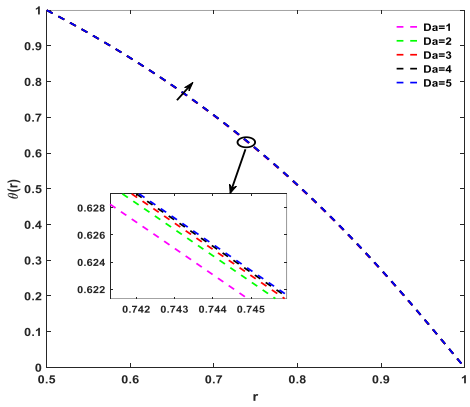

Figure 9. Variation of Da with temperature.

3.5. Effect of Reynolds number (Re).

Impact of Reynolds number on velocity and temperature profiles is visualized in Figures 10 and 11 as the Reynolds number increases, both velocity and temperature increase. In Figure 10, velocity increases due to the dominance of inertial forces, mixing effects of transition flows, and the magnetic force. Temperature increases as the Reynolds number increases because the fluid's kinetic energy is dissipated, it converts thermal energy into chaotic motion, and its thermal conductivity increases. In the design of automobiles, a compressor is used.

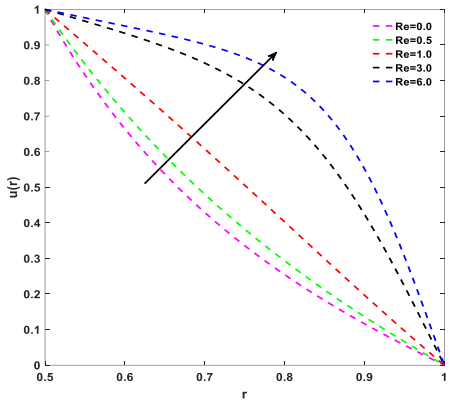

Figure 10. Variation of Re on velocity.

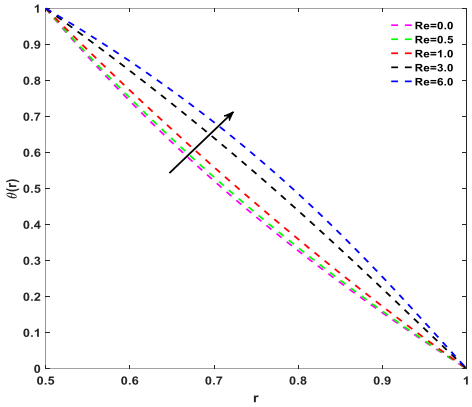

Figure 11. Variation of Re with temperature.

3.6. Effect of radiation parameter (N).

Influence of radiation on the temperature graph observed in Figure 12: as radiation increases, temperature decreases. This is because the system radiates more thermal energy, leading to a decrease in the overall system's internal energy, which is used in cooling systems. Figure 13 shows the Nusselt number versus Hartmann number for different values of radiation effects. As the Nusselt number increases, the wall temperature increases due to friction between the fluid and the cylinder wall. Variation of velocity of different nanoparticles is observed in Figure 14, as H_2O -Ag has a higher velocity than H_2O-Cu and H_2O -CuO because the density and viscosity are higher for Ag than Cu and CuO. From Figure 15, it is observed that the temperature is higher for H_2O -CuO than H_2O -Ag and H_2O -Cu due to the higher thermal conductivity of CuO, Ag, and Cu. Table 3 [30] shows the validation of the velocity and temperature graphs results when $Q = 0, Da = 0.001$ $\phi = 0.01, Pr = 6.8, Ec = 0.1, N = 0.2, Re = 1, Ha = 1$, are in good agreement with the existing work of Peng *et al.* [30].

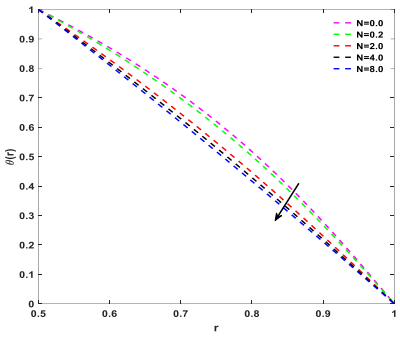

Figure 12. Variation of N with temperature.

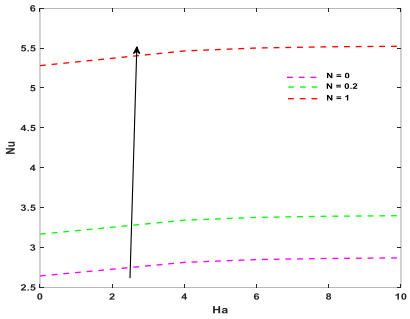

Figure 13. Effect of Nusselt number and Hartmann number on radiation.

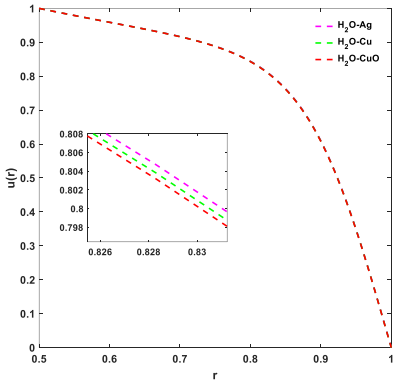

Figure 14. Variation of different nanoparticles on velocity.

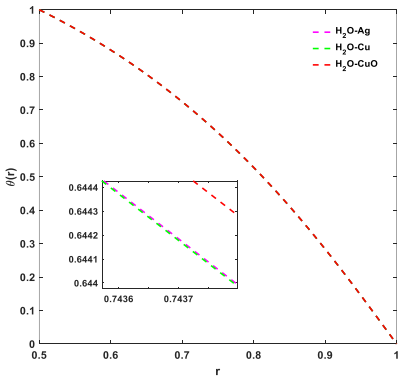

Figure 15. Variation of different nanoparticles with temperature.

3.7. Effect of aspect ratio (η).

The influence of aspect ratio η on the velocity and temperature in Figures 16 and 17, distributions in MHD nanofluid flow within a concentric cylindrical system. As η increases, indicating a narrower gap between the cylinders, the velocity profile shows a steeper gradient

and a sharper drop near the outer boundary. This occurs because the reduced flow domain constrains the fluid motion, leading to increased shear and reduced overall velocity. The narrowing of the annular space alters the flow dynamics significantly, concentrating the velocity closer to the inner wall. Similarly, the temperature profile decreases slightly with increasing η. A higher aspect ratio results in a smaller fluid volume between the cylinders, limiting convective heat transfer and reducing thermal energy distribution. This geometric constraint leads to lower temperature values throughout the flow domain. These observations are particularly relevant in biomedical applications such as cancer hyperthermia, where careful tuning of the aspect ratio allows precise control of heat distribution and fluid behaviour to maximize therapeutic efficiency while protecting surrounding healthy tissues. Figure 18 compares the temperature profiles for two thermal-conductivity models, the Patel and Maxwell-Garnett models, as the radiation parameter increases in an MHD nanofluid flow through a concentric cylinder. As N increases, the temperature distribution decreases across the radial domain, indicating that stronger thermal radiation leads to enhanced heat loss from the system.

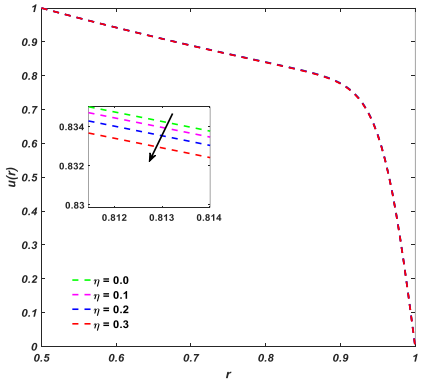

Figure 16. Variation of η on velocity.

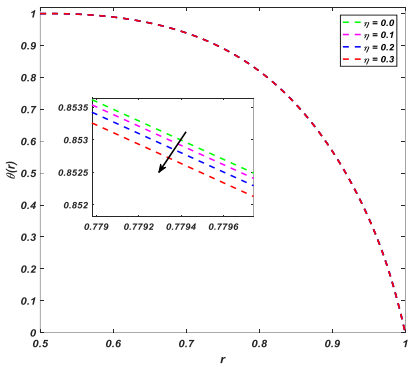

Figure 17. Variation of η with temperature.

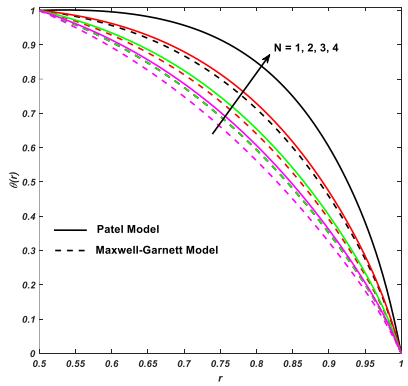

Figure 18. Comparison of thermal conductivity models.

3.8. Effect of Nusselt number (Nu) and skin friction (C_f).

Effects of Nusselt number (Nu) and Skin friction (C_f) are explained for different parameters plotted in Figures 19, 20 (a and b). Figure 19 (a and b) represents the influence of the Harmann number versus skin friction for varying Reynolds number, observed Re increases, temperature, and velocity decreases at the wall. Viscous dissipation effect and internal heat source parameter are drawn graphically in Figure 20 (a and b). It shows that an increasing Ec value increases Nu, and an opposite trend is observed in Q values. Nu is decreasing, which means the intensity is more.

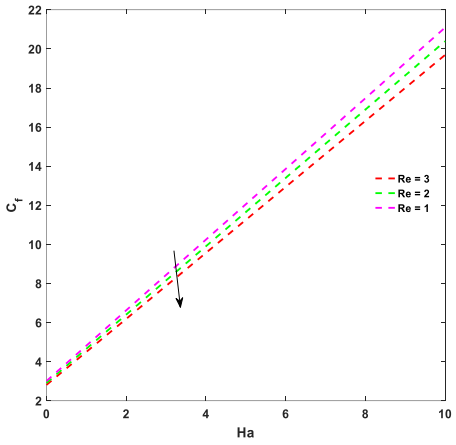

Figure 19. Effect of Skin friction and Hartmann number on Renolds number.

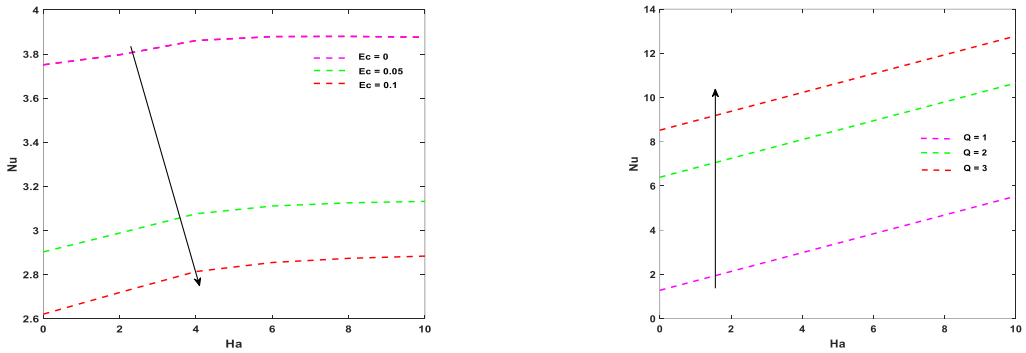

(a) **(b)**

Figure 20. Effect of Nusselt number and Hartmann number on **(a)** Ec; **(b)** Q.

Table 3. Validation of the work for velocity and temperature Re=1, Ha=1, Ec=0.1, N=0.2, Da=0.001, Q=0.

r	Velocity	Present study	Temperature	Present study
0.500000000	1.000000000	1.000000000	1.000000000	1.000000000
0.507264546	0.977304817	0.977304814	1.000108603	1.000108605
0.528635994	0.912982911	0.912982920	0.996313234	0.996313236
0.562872313	0.816808808	0.816808809	0.978284458	0.978284459
0.607983813	0.701138961	0.701138963	0.934310258	0.934310260
0.661348778	0.577709577	0.577709579	0.856439761	0.856439763
0.719865830	0.455903028	0.455903030	0.744091562	0.744091566
0.780134170	0.342414779	0.342414781	0.605066162	0.605066167
0.838651222	0.241687777	0.241687780	0.453613121	0.453613124
0.892016187	0.156563181	0.156563184	0.306434992	0.306434995
0.937127687	0.088853094	0.088853096	0.178594509	0.178594510
0.971364006	0.039734716	0.039734717	0.081084505	0.081084507
0.992735454	0.009896650	0.009896651	0.020495729	0.020495730
1.000000000	0.000000000	0.000000000	0.000000000	0.000000000

4. Conclusions

This study considered fully developed mixed convection flow of nanofluids, incompressible steady, laminar flow over two concentric cylinders, heat generation, and MHD porous matrix in the presence of solar radiation. The effects of volume fraction, Hartmann number, thermal radiation parameter, internal heat source parameter, Darcy effect, and Reynolds number are analyzed. The main outcome of this work is that thermal radiation reduces the temperature gradient within the annulus, leading to a uniform temperature distribution across the flow. The impact of MHD effects on the nanofluid flow patterns diminishes the fluid flow rate and stabilizes the magnetic field strength. Porous medium acts as a resistance to the flow, influenced by thermal radiation and Lorentz force. The combined effects of internal heat generation, thermal radiation, and MHD intensify the increased temperature and thermal boundary layer. The study of MHD, thermal radiation, internal heat sources, and porous nanofluids in an annulus is essential for applications in industries such as energy, aerospace, materials processing, rotating machinery, and heat exchangers.

Author Contributions

Conceptualization, M. R. and S. K. T.; methodology, M. R. and S. K. T.; software, M. R. and S. K. T.; validation, M. R., S. K. T., and N. N.; formal analysis, M. R., S. K. T., and N. N.; investigation, M. R., S. K. T., and S. R.; resources, M. R. and S. K. T.; data curation, M. R. and S. K. T.; writing—original draft preparation, M. R., S. K. T., and N. N.; writing—review and editing, M. R. and S. K. T.; visualization, M. R. and S. K. T.; supervision, S. K. T. and N. N. All authors have read and agreed to the published version of the manuscript.

Institutional Review Board Statement

Not applicable.

Informed Consent Statement

Not applicable.

Data Availability Statement

The complete data is available in the main text.

Funding

This research received no external funding.

Acknowledgments

The authors are grateful to the Research Center at Atria Institute of Technology for their support and encouragement in conducting our research.

Conflicts of Interest

The authors declare no conflict of interest.

Abbreviations

The following abbreviations are used in this manuscript:

Abbreviation	Definition
B_0	Magnetic Field Strength, T
Cp	Specific Heat $(kJ/kg.K)$
Da	Darcy Effect
Ec	Eckert Number
Ha	Hartmann Number
N	Radiation Parameter
Nu	Nusselt Number
Pr	Prandtl Number
Q	Internal Heat Source/Sink Parameter
q_r	Radiative Heat Flux
R	Radial Axis
Re	Renolds Number
r_1	Radius of the Inner Cylinder, (m)
r_2	Radius of the Outer Cylinder, (m)
T	Dimensional temperature (K)
U	Dimensional Velocity, (ms^{-2})
u	Dimensional Velocity, (ms^{-2})
ω	Constant Rotation Velocity, (rad/s)
α	Thermal Diffusivity, (m^2/s)
ϕ	Solid Volume Fraction
μ	Dynamic Viscosity, $(Pa.s)$
ρ	Density, (kg / m^3)
η	Aspect Ratio
θ	Dimensionless Temperature (K)
υ	Kinematic Viscosity, (m^2/s)
κ	Thermal Conductivity of Fluid. (W/m. K)
β	Thermal Expansion Coefficients. (K^{-1})
σ	Electrical Conductivity, (S/m)
θ	Dimensionless Temperature
nf	Nanofluid
f	Base Fluid
s	Solid Nanoparticles

References

1. Choi, S.U.S.; Eastman, J.A. Enhancing thermal conductivity of fluids with nanoparticles. Proceedings of the ASME International Mechanical Engineering Congress and Exposition, San Francisco, CSA, USA, 12-17 November 1995; **1995**.
2. Merkin, J.H.; Roșca, N.C.; Roșca, A.V.; Pop, I. MHD Mixed Convection Flow Over a Permeable Vertical Flat Plate Embedded in a Darcy–Forchheimer Porous Medium. *Transp. Porous Med.* **2024**, *151*, 2511-2528, https://doi.org/10.1007/s11242-024-02124-6.
3. Ali, A.; Das, S.; Muhammad, T. Dynamics of blood conveying copper, gold, and titania nanoparticles through the diverging/converging ciliary micro-vessel: Further analysis of ternary-hybrid nanofluid. *J. Mol. Liq.* **2023**, *390*, 122959, https://doi.org/10.1016/j.molliq.2023.122959.
4. Gurejala, J.R.; Vadla, D.G.K.; Mella, D.A.K. The *pdepe* solver for analysing the flow of MHD Cu-H_2O nanofluid across an oscillating vertical plate. *Case Stud. Chem. Environ. Eng.* ***2024***, *10*, 100910, https://doi.org/10.1016/j.cscee.2024.100910.
5. Uddin, M.J.; Hasan, M.M.; Faroughi, S.A. Convective transport in a nanofluid-filled annulus with an eccentric hypocycloid within a square disk. *Int. J. Thermofluids* **2024**, *22*, 100664, https://doi.org/10.1016/j.ijft.2024.100664.
6. Ali, A.; Das, S. Applications of neuro-computing and fractional calculus to blood streaming conveying modified trihybrid nanoparticles with interfacial nanolayer aspect inside a diseased ciliated artery under electroosmotic and Lorentz forces. *Int. Commun. Heat Mass Transf.* **2024**, *152*, 107313, https://doi.org/10.1016/j.icheatmasstransfer.2024.107313.

7. Das, S.; Sarkar, S.; Ali, A.; Nath Jana, R. Exploration of magnetically influenced flow dynamics of a dusty fluid induced by the ramped movement of a thermally active plate. *Arch. Appl. Mech.* **2024**, *94*, 407-433, https://doi.org/10.1007/s00419-023-02531-z.
8. Abdelmalek, Z.; Rehman, K.U.; Al-Mdallal, Q.M.; Al-Kouz, W.; Malik, M.Y. Dynamics of thermally magnetized grooved flow field having uniformly heated circular cylinder: Finite element analysis. *Case Stud. Therm. Eng.* **2020**, *21*, 100718, https://doi.org/10.1016/j.csite.2020.100718.
9. Saranya, S.; Al-Mdallal, Q.M. Non-Newtonian ferrofluid flow over an unsteady contracting cylinder under the influence of aligned magnetic field. *Case Stud. Therm. Eng.* **2020**, *21*, 100679, https://doi.org/10.1016/j.csite.2020.100679.
10. Vahidi, J.; Akbari, H.; Ghasemi, S.E. An optimal analytical study on a solar photovoltaic system with different rates of absorbed photon and emitted electron. *Results Eng.* **2023**, *20*, 101634, https://doi.org/10.1016/j.rineng.2023.101634.
11. Besthapu, P.; F, M.; Shanker, B.; Alfunsa, P. Analysis of convective heat transfer in triple diffusive free convection flow of Williamson nanofluid along a horizontal plate. *Int. J. Model. Simul.* **2025**, *45*, 1506-1515, https://doi.org/10.1080/02286203.2023.2288773.
12. Gouran, S.; Vahidi, J.; Akbari, H.; Ghasemi, S.E. Thermal radiation and porous medium effects on a thin liquid film over a stretching sheet: A numerical comparative study. *Case Stud. Therm. Eng.* **2023**, *52*, 103753, https://doi.org/10.1016/j.csite.2023.103753.
13. Saranya, S.; Al-Mdallal, Q.M.; Javed, S. Shifted Legendre Collocation Method for the Solution of Unsteady Viscous-Ohmic Dissipative Hybrid Ferrofluid Flow over a Cylinder. *Nanomaterials* **2021**, *11*, 1512, https://doi.org/10.3390/nano11061512.
14. Ghasemi, S.E.; Ranjbar, A.A. Three-dimensional numerical simulation of a laminar fluid flow in an enhanced microchannel with circular protrusions. *Math. Method. Appl. Sci.* **2025**, *48*, 7651-7660, https://doi.org/10.1002/mma.9245.
15. Ghasemi, S.E.; Gouran, S. Mathematical simulation of laminar micropolar fluid flow between two disks for two different geometries. *Waves Random Complex Media* **2023**, 1-22, https://doi.org/10.1080/17455030.2023.2182139.
16. Dehghani, M.R.; Kafi, M.; Nikravesh, H.; Aghel, M.; Mohammadian, E.; Kazemzadeh, Y.; Azin, R. Data driven models for predicting pH of CO_2 in aqueous solutions: Implications for CO_2 sequestration. *Results Eng.* **2024**, *24*, 102889, https://doi.org/10.1016/j.rineng.2024.102889.
17. Gouran, S.; Ghasemi, S.E. Thermal analysis of rectangular moving fins with temperature-variant properties by employing the Galerkin scheme. *Heat Tranf.* **2024**, *53*(5), 2281-2293, https://doi.org/10.1002/htj.23039.
18. Vahidi, J.; Akbari, H.; Ghasemi, S.E. A new computational approach for velocity components analysis of a solid particle in an incompressible fluid flow. *Int. J. Mod. Phys. C* **2023**, *35*, 2450049, https://doi.org/10.1142/s0129183124500499.
19. Ghasemi, S.E.; Valipour, P.; Hatami, M.; Ganji, D.D. Heat transfer study on solid and porous convective fins with temperature-dependent heat generation using efficient analytical method. *J. Central South Univ.* **2014**, *21*, 4592-4598, https://doi.org/10.1007/s11771-014-2465-7.
20. Ghasemi, S.E.; Hatami, M.; Ganji, D.D. Thermal analysis of convective fin with temperature-dependent thermal conductivity and heat generation. *Case Stud. Therm. Eng.* **2014**, *4*, 1-8, https://doi.org/10.1016/j.csite.2014.05.002.
21. Talarposhti, R.A.; Ghasemi, S.E.; Rahmani, Y.; Ganji, D.D. Application of Exp-function method to wave solutions of the Sine-Gordon and Ostrovsky equations. *Acta Math. Appl. Sin. Engl. Ser.* **2016**, *32*, 571-578, https://doi.org/10.1007/s10255-016-0571-z.
22. Sheikholeslami, M.; Nimafar, M.; Ganji, D.D. Nanofluid heat transfer between two pipes considering Brownian motion using AGM. *Alex. Eng. J.* **2017**, *56*, 277-283, https://doi.org/10.1016/j.aej.2017.01.032.
23. Sohail, M.; Naz, R.; Shah, Z.; Kumam, P.; Thounthong, P. Exploration of temperature dependent thermophysical characteristics of yield exhibiting non-Newtonian fluid flow under gyrotactic microorganisms. *AIP Adv.* **2019**, *9*, 125016, https://doi.org/10.1063/1.5118929.
24. Sohail, M.; Naz, R. Modified heat and mass transmission models in the magnetohydrodynamic flow of Sutterby nanofluid in stretching cylinder. *Phys. A Stat. Mech. Appl.* **2020**, *549*, 124088, https://doi.org/10.1016/j.physa.2019.124088.
25. Ghasemi, S.E.; Hatami, M. Solar radiation effects on MHD stagnation point flow and heat transfer of a nanofluid over a stretching sheet. *Case Stud. Therm. Eng.* **2021**, *25*, 100898, https://doi.org/10.1016/j.csite.2021.100898.

26. Shikholeslami, M. Magnetic source impact on nanofluid heat transfer using CVFEM. *Neural Comput. Appl.* **2018**, *30*, 1055–1064, https://doi.org/10.1007/s00521-016-2740-7.
27. Sheikholeslami, M. Investigation of Coulomb force effects on ethylene glycol based nanofluid laminar flow in a porous enclosure. *Appl. Math. Mech.* **2018**, *39*, 1341–1352, https://doi.org/10.1007/s10483-018-2366-9.
28. Valipour, P.; Ghasemi, S.E.; Vatani, M. Theoretical investigation of micropolar fluid flow between two porous disks. *J. Central South Univ.* **2015**, *22*, 2825-2832, https://doi.org/10.1007/s11771-015-2814-1.
29. Gouran, S.; Mohsenian, S.; Ghasemi, S.E. Theoretical analysis on MHD nanofluid flow between two concentric cylinders using efficient computational techniques. *Alex. Eng. J.* **2022**, *61*, 3237-3248, https://doi.org/10.1016/j.aej.2021.08.047.
30. Peng, Y.; Alsagri, A.S.; Afrand, M.; Moradi, R. A numerical simulation for magnetohydrodynamic nanofluid flow and heat transfer in rotating horizontal annulus with thermal radiation. *RSC Adv.* **2019**, *9*, 22185-22197, https://doi.org/10.1039/c9ra03286j.
31. Sravan Kumar, T.; Dinesh, P.A.; Makinde, O.D. Impact of Lorentz Force and Viscous Dissipation on Unsteady Nanofluid Convection Flow over an Exponentially Moving Vertical Plate. *Math. Models Comput. Simul.* **2020**, *12*, 631-646, https://doi.org/10.1134/s2070048220040110.
32. Sushma, T.C.; Nalinakshi, N.; Dinesh, P.A.; Jayalakshmamma, D.V.; Sravan Kumar, T. Convective heat transfer and MHD flow through semi-porous cylindrical filters embedded in an impermeable region. *Chin. J. Phys.* **2023**, *81*, 9-25, https://doi.org/10.1016/j.cjph.2022.10.015.
33. Kavitha, S.; Nalinakshi, N.; Dinesh, P.A.; Brijesh. Analysis of Forchheimer Effect for Double Diffusive Convection With Dusty Fluids and MHD. *J. Mines Met. Fuels* **2023**, *71*, 2289-2299, https://doi.org/10.18311/jmmf/2023/36331.
34. Patel, H.E.; Anoop, K.B.; Sundararajan, T.; Das, S.K. A MICRO-CONVECTION MODEL FOR THERMAL CONDUCTIVITY OF NANOFLUIDS. Proceedings of the International Heat Transfer Conference 13, Sydney, Australia, 13-18 August 2006; Begel House Inc.: **2006**; https://doi.org/10.1615/ihtc13.p8.240.
35. Mebarek-Oudina, F. Cross-diffusion effects on an MHD Williamson nanofluid flow past a nonlinear stretching sheet immersed in a permeable medium. *Front. Heat Mass Transf.* **2024**, *22*, 15–34, https://doi.org/10.32604/fhmt.2024.048045.
36. Madan Kumar, R.; Srinivasa Raju, R.; Anil Kumar, M. Effects of chemical reaction, Soret and Dufour parameters on MHD dissipative Williamson nanofluid flow over a slippery stretching sheet through a porous medium. *Int. J. Model. Simul.* **2025**, *45*, 1135-1145, https://doi.org/10.1080/02286203.2023.2261812.
37. Venkatesh, N.; Srinivasa Raju, R.; Anil Kumar, M.; Vijayabhaskar, C. Heat and mass transfer in Maxwell fluid with nanoparticles past a stretching sheet in the existence of thermal radiation and chemical reaction. *Int. J. Model. Simul.* **2025**, *45*, 1200-1213, https://doi.org/10.1080/02286203.2023.2266798.
38. Das, S.; Banu, A.S.; Sarkar, S.; Ali, A.; Jana, R.N. Intricate dynamics of rotational buoyancy, magnetic field, Hall current, and infrared radiation in a Casson fluid medium. *Z. Angew. Math. Mech.* **2024**, *104*, e202300657, https://doi.org/10.1002/zamm.202300657.
39. Ali, A.; Mebarek-Oudina, F.; Barman, A.; Das, S.; Ismail, A.I. Peristaltic transportation of hybrid nano-blood through a ciliated micro-vessel subject to heat source and Lorentz force. *J. Therm. Anal. Calorim.* **2023**, *148*, 7059-7083, https://doi.org/10.1007/s10973-023-12217-x.
40. Ali, A.; Das, S.; Jana, R.N. MHD gyrating stream of non-Newtonian modified hybrid nanofluid past a vertical plate with ramped motion, Newtonian heating and Hall currents. *Z. Angew. Math. Mech.* **2023**, *103*, e202200080, https://doi.org/10.1002/zamm.202200080.

Publisher's Note & Disclaimer

information before relying on it, and the publisher assumes no responsibility for any consequences arising from the use of materials contained in this publication.